CHEMICAL ENGINEERING TRANSACTIONS
VOL. 69, 2018
A publication of AIDIC
The Italian Association of Chemical Engineering
Online at www.aidic.it/cet
Guest Editors: Elisabetta Brunazzi, Eva Sorensen

ISBN 978-88-95608-66-2; **ISSN** 2283-9216
DOI: 10.3303/CET1869011

Direct Numerical Simulations of Liquids on Microstructured Surfaces: Analysing the Fluid Dynamics on Packing

Henning Bonart*, Jens-Uwe Repke

Technische Universität Berlin, Straße des 17. Juni 135, 10623 Berlin, Germany
henning.bonart@tu-berlin.de

Structured high performance packing for packing columns have macrostructures, e.g., corrugated or folded sheets, and in many cases microstructures or surface topographies with geometrical dimensions in the same order of magnitude as the film thicknesses. For an optimal design of microstructured surfaces and for the development of novel methodologies to predict the mass transfer, a reliable description of the influence of these microstructures is crucial. To research the influence of these microstructures on the liquid film in detail, and later on optimize the geometry, Direct Numerical Simulations applying the Cahn-Hilliard-Navier-Stokes (CHNS) equations were performed for this study. The model and the implementation were validated against analytical solutions for undisturbed laminar film flows. The influence of two single microstructures (triangle and rectangle) on the gas-liquid interface and the velocity in the liquid were systematically investigated. Thereby, it was observed, that small microstructures in comparison to the film thickness have no influence on the gas-liquid interface. In contrast, higher structures could increase the interfacial area. The results indicate, that systematic studies on a wide range of geometries, phase properties and gas velocities can give valuable information on the path to optimal microstructures.

1. Introduction

Structured high performance packing for packing columns have macrostructures, e.g., corrugated or folded sheets, and in many cases microstructures or surface topographies with geometrical dimensions in the same order of magnitude as the film thicknesses to enhance the wetting behavior. The characterization of the transport phenomena, i.e., momentum, mass and heat, in these liquid film flows over these microstructured surfaces are of great importance for chemical engineering applications like distillation and absorption processes. It is needed for the optimal design of the texture on the packing surface and for the optimal selection of a packing for a specific separation task as well as for the development of novel methodologies to predict the mass transfer parameters (Repke, 2011). However, a reliable and comprehensible description of the influence of these microstructures on the mass- and heat transfer between gas and liquid film is still missing.
In contrast to the macrostructures, the emphasis on overflown or surrounded, single microstructures is rarely found in the literature. In (Dressaire et al., 2010) the influence of the geometry of cylinders on the structure of the fluid film was investigated. An influence of triangular pyramids on the surface velocity was found by (Paschke, 2011). A significant intensification of the mass transfer due to the texture design of up to 80% compared to a flat inclined plate was found by (Kohrt, 2011). In (Kapoustina et al., 2015) the spatial distribution of absorbed gas into the film flow disturbed by a micropyramid was researched and an enhancement of the mass transport due to the microstructure was shown. In addition to experiments, numerical simulations allow an even deeper insight into the fluid dynamics of liquid films. Thereby, the usage of the complete Navier-Stokes equations for both gas and liquid phase or Direct Numerical Simulation (DNS) allows to simulate complex, three dimensional geometries with sharp edges and higher Reynolds numbers (Veremieiev et al, 2015). DNS resolve all length and time scales including swirls, boundary layers, and the gas-liquid interface (Ferziger, 2002). In (Gambaryan-Roisman et al., 2005) the effect of a sinusoidal surface structure was described. A sharp step was investigated in (Bontozoglou and Serifi, 2008) and the influence of

Please cite this article as: Bonart H., Repke J.U., 2018, Direct numerical simulations of liquids on microstructured surfaces: analyzing the fluid dynamics on packing, Chemical Engineering Transactions, 69, 61-66 DOI: 10.3303/CET1869011

inertia was discussed. Three dimensional simulations over two types of microstructures were performed in (Veremieiev, 2010) but they neglected the gas phase.
However, the influence of microstructures on the interfacial area and subsequently on the mass transport is not fully understood yet. Although it is known that single microstructures do have an effect on the dynamics and transport phenomena in the liquid film and the overflowing gas phase, little information is available for the systematic selection of microstructures on surfaces, e.g., for structured high performance packings. Therefore, in this paper first steps for the systematic DNS based research on film flows over microstructures are presented. For the description of the two phase flow, the Cahn-Hilliard-Navier-Stokes model is applied and briefly described in Chapter 2. To the authors' knowledge, this is the first application of the CHNS model for film flows. Afterwards, the test case including mesh and boundary conditions is presented. After a brief but significant validation of both the model and implementation, the results of 20 different configurations including two different microstructures are compared and discussed in Chapter 3. Finally, a conclusion and an outlook is given.

2. Methodology

2.1 Cahn-Hilliard-Navier-Stokes

To model the two phase film flow, the common incompressible, single-field Navier-Stokes (NS) equation is combined with the convective Cahn-Hilliard (CH) equation to describe the interface dynamics. The CHNS equations can be derived purely from thermodynamic principles (Abels, 2012). Diffuse interface methods replace the infinitely thin boundary between gas and liquid by a transition region with finite thickness. It follows, that all physical properties like density or viscosity vary continuously across the interface. The diffuse gas-liquid interface makes explicit tracking of the interface unnecessary. All governing equations are solved as single-field equations, i.e., no jump conditions between the two phases are needed (Wörner, 2012). The position of the interface is then implicitly given by the phase field. One of the major advantages is, that the formulation of the surface tension force f=-μ∇ϕ in the NS equation exactly conserves both the surface tension energy and kinetic energy. This can reduce spurious currents, which are purely artificial velocities around the interface, to the level of the truncation error even for low Capillary numbers (He and Kasagi, 2008). Here, the thermodynamically consistent diffuse interface model for large density differences between gas and liquid by (Abels, 2012) was applied:

$$\rho\partial_t u + \left(\left(\rho u + J\right)\cdot\nabla\right)u - \nabla\cdot\left(2\eta Du\right) + \nabla p = -\mu\nabla\varphi + \rho g \tag{1}$$

$$\nabla\cdot u = 0 \tag{2}$$

$$\partial_t\varphi + \left(u\cdot\nabla\right)\varphi = m\nabla^2\mu \tag{3}$$

$$\mu = -\sigma\varepsilon\nabla^2\varphi + \sigma W'\left(\varphi\right)/\varepsilon\,, \tag{4}$$

in which u and p are the velocity and pressure, ρ and η are the mixture density and viscosity and g is the gravitational constant. Furthermore, σ is a scaled surface tension and μ is a chemical potential. The phasefield ϕ acts as an order parameter to describe the distribution of liquid and gas. The parameter m is a diffusion coefficient for the interface, W is a relaxed double obstacle free energy density and ε describes the interface thickness. Furthermore, J stems from the mass conservation for different densities in gas and liquid and Du is the symmetrized velocity gradient.
The CHNS equations form a very tightly coupled and highly nonlinear system of four partial differential equations. Furthermore, the Cahn-Hilliard Equation 3 together with Equation 4 involves fourth-order derivatives with respect to ϕ. Compared to the NS Equations 1 and 2, which involve only second-order derivatives, this complicates the numerical treatment (Wörner, 2012). To enable the efficient solution, the solution scheme from (Garcke et al., 2016) was implemented into the Finite-Element toolbox FEniCS (Alnaes et al., 2015). For the solution of the resulting nonlinear equation system, PETSc (Balay et al., 2014) and SuperLU_dist (Li et al., 2011) were applied, see (Bonart, 2017). All simulations were performed on the supercomputer Konrad of HLRN (North-German Supercomputing Alliance).

2.2 Test case

In Figure 1a the simulation domain is shown. On the top and bottom wall no-slip boundary conditions were used. Furthermore, periodic boundary conditions were assumed on the left and right side of the domain. In this way, the flow leaving the domain through the right boundary is identical to the flow entering the domain on the left side (Ferziger, 2002). The front and back of the domain were assumed to be symmetric. Furthermore, velocity components transverse to the main flow direction were neglected. Subsequently, only two dimensional simulations were performed for this paper but the methodology will be extended to three dimensions. Similar to a packing column, the flow was purely driven by gravity, i.e., ρg in the NS-equations, with the gravitational acceleration constant g. The height and length of the domain was 4 respectively 16 times the particular film thickness. This reduced the effects of the upper wall on the film flow and allowed the liquid film to settle down after being disturbed by the obstacle. Exemplary, a triangular obstacle with base length and height of 0.8 times the film thickness is shown in Figure 1a. Figure 1b shows an excerpt of a mesh. The unstructured meshes were generated using mshr and CGAL and consisted of around 110,000 triangles, which was found to sufficiently resolve both the wall boundary layers and the gas-liquid interface.

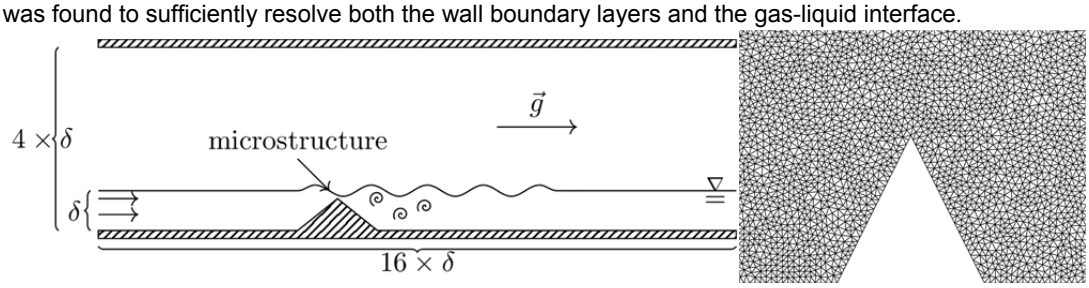

Figure 1: Illustration of the considered test configuration (left, a) and an excerpt of the computational mesh used for the simulations with a triangular obstacle (right, b)

To characterize the range of flows used in the simulations, several dimensionless numbers and characteristic quantities are given in Table 1. For low Reynolds numbers Re both the mean velocity v and the film thickness take low values. In addition, the Capillary number Ca and the Bond number Bo are small too. This implies, that the viscous forces across the interface respectively the gravitational forces are much more important for the flow than the surface tension forces. Subsequently, the surface tension forces have more impact for higher Re. Note, that the Atwood number At indicates a large density ratio between liquid and gas. In this way, the influence of the gas flow on the liquid is reduced.

Table 1: Dimensionless numbers and characteristic quantities

$\mathrm{Re} = \frac{UL}{\nu_l}$	$At = \frac{(\rho_l - \rho_v)}{(\rho_l + \rho_v)}$	$Ca = \frac{(\nu_l \rho_l U)}{\sigma}$	$Bo = (\rho_l - \rho_g)\frac{gL^2}{\sigma}$	$L(m)$	$U(m/s)$
0.25 - 4.0	0.99	0.024 - 0.15	0.07 - 0.45	δ	$\bar{u}$

3. Simulations

3.1 Laminar liquid film on a smooth plate

In a first step, the model and implementation were validated against analytical results derived by Nusselt for laminar liquid film flows on smooth plates with insignificant influence of the gas phase, see (Spurk and Aksel, 2008). Therefore, simulations with five different Reynolds numbers between 0.25 and 4.0 were carried out until a steady state was reached. The initial film thickness was calculated from the Reynolds number Re by

$$\delta = \left(3\frac{\nu^2}{g}\mathrm{Re} \right)^{1/3}, \tag{5}$$

where ν is the kinematic viscosity. In Figure 2a, a simulated velocity profile is plotted against the analytical velocity profile calculated by

$$u_x(y) = \frac{3}{2}\left(2\frac{y}{\delta} - \left(\frac{y}{\delta}\right)^2\right)\bar{u}_x \text{ , where } \bar{u}_x = \left(\frac{\nu}{(3g)}\mathrm{Re}^2\right)^{1/3} . \quad (6)$$

It is obvious, that the simulated velocity profile agrees very well with the analytical solution. In addition, Figure 2b shows the maximum of the velocity from the simulations against the analytical solution for the whole range of Reynolds numbers. Again, the simulation is in excellent agreement with the analytical results. It is concluded, that the model and the implementation are capable of simulating two-phase film flows.

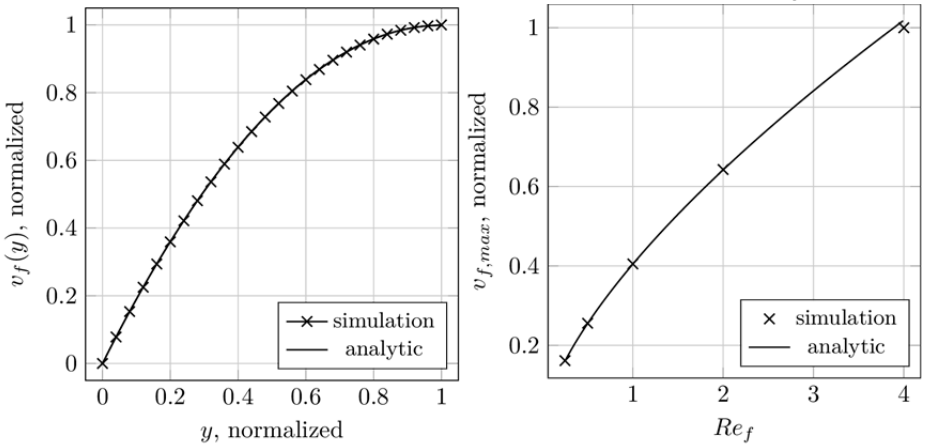

Figure 2: Simulated and analytic velocity profile normal to the wall for Re=2.0 (left, a) and the simulated and analytic maximal film velocities for several Re (right, b) on a smooth plate. All values are normalized to the maximum value

3.2 Liquid film over single microstructures

For the simulations of liquid films over single microstructures, the same test configuration as before was used. The laminar, undisturbed film flow was applied as the initial condition and the same Reynolds numbers as before were simulated (Re=0.25-0.4). The mesh was altered to include the obstacles. Exemplarily, a rectangle and triangle in two different sizes, e.g., 0.2 and 0.8 times the particular film thickness δ, were chosen for this study. In total 20 simulations were performed (2 different geometries with two different heights for 5 different Reynolds numbers). All simulations were performed until a steady or periodic flow, i.e., waves, were reached.

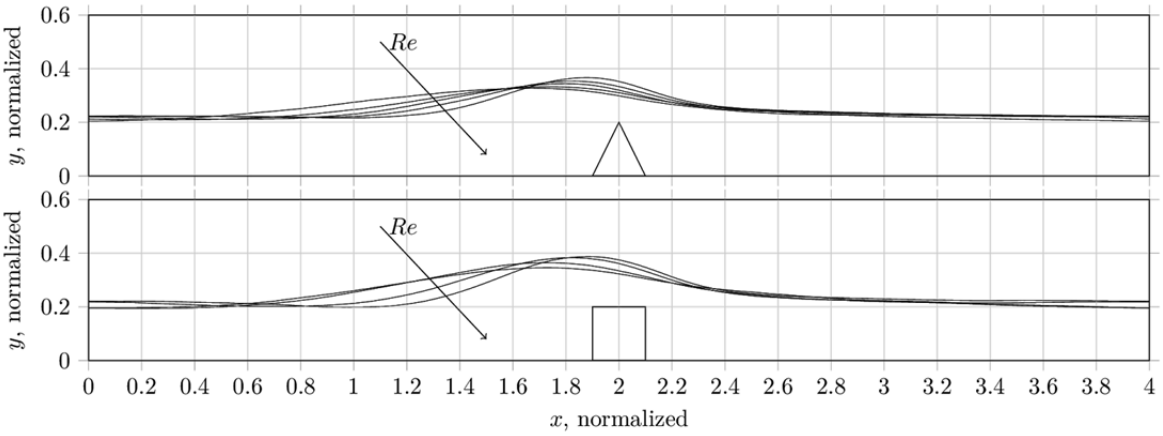

Figure 3: Disturbed interfaces between liquid film and gas. The height of the obstacles is 0.8δ. All coordinates are normalized to the particular film thickness δ

Figure 3 shows the interface between liquid and gas for the two obstacles with size 0.8δ at different Reynolds numbers. To allow the direct comparison, the geometrical dimensions are normalized to the particular film thickness. It is clearly visible, that both obstacles disturb the liquid film in a similar way: upstream of the obstacles, the film is retained and the film thickness gets larger because of the redirection of the film across

the obstacle. Behind the obstacle, the disturbance dissipates and the undisturbed film thickness is reached again in almost all cases. For higher Reynolds numbers (or higher inertia compared to viscous forces), the maximum film thickness gets larger and the position of the maximum is more near the obstacles whereas for low Reynolds numbers the impounding begins further upstream, compare (Veremieiev et al, 2015). Comparing the effects of the two obstacle geometries, it is noted, that the effect of the rectangular obstacle on the interphase is slightly stronger. Figure 4 plots the velocity streamlines for both obstacles with h=0.8δ and Re=4.0. In contrast to the triangular obstacle, a small recirculation zone is formed behind the rectangular obstacle.

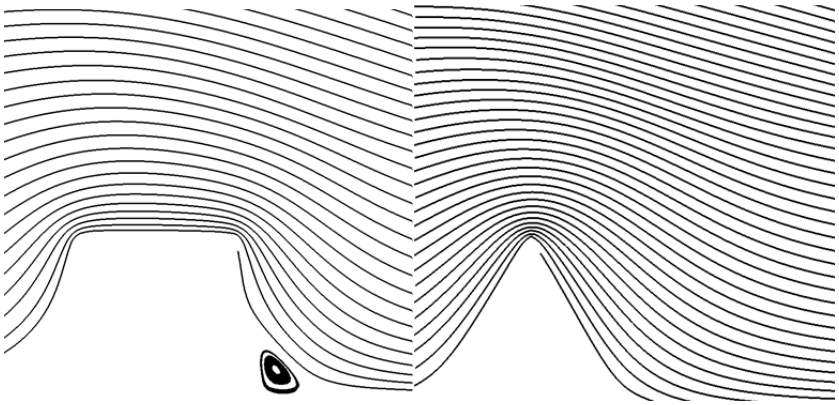

Figure 4: Velocity streamlines for rectangular (left) and triangular obstacle with h=0.8δ and Re=0.4

To allow the evaluation of the obstacles concerning the disturbance of the interfacial area (or length of the interface since only two dimensional simulations are used yet), Figure 5 shows the lengths of the simulated interfaces normalized with the particular interfacial lengths of the undisturbed film flows. It is clearly visible, that for small heights, i.e., 0.2δ, the interface shows practically no changes compared to the undisturbed film for both obstacles. In contrast, the interfacial lengths are larger for both obstacles with 0.8δ with a stronger influence by the rectangular obstacle. Furthermore, the interfacial lengths exhibit a clear dependency on the Reynolds number, i.e., the interfacial length gets larger for higher Reynolds numbers. Consequential, the mass transfer should be enhanced for higher Reynolds numbers too due to the resulting higher mass transfer area provoked by the microstructures.

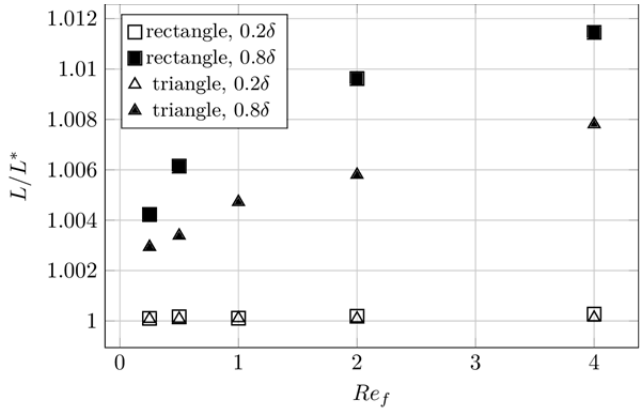

Figure 5: Length of the interfaces between liquid film and gas for different obstacles and Re. The lengths are normalized to the undisturbed interface length

4. Conclusions

To enhance the understanding of the physical phenomena in disturbed liquid film flows on packing surfaces, such as mass transfer, a reliable description of the influence of microstructures on the liquid film is crucial. Furthermore, this can help to design optimal microstructured surfaces and enable the systematic selection of geometries for specific separation tasks. However, little information is available on the influence of such microstructures on the liquid film. In this paper, the complex CHNS model was applied to describe the two phase flow and the motion of the interface in great detail. One of the major advantages of the CHNS model is,

that even for very low Capillary numbers spurious currents are greatly reduced. Consequently, the model allows the simulation of very thin films over small microstructures. To the authors' knowledge, this is the first application of the CHNS model for periodic filmflows. The model and Finite-Element implementation were successfully validated against analytical results of undisturbed film flows. Subsequently, in total 20 simulations in 2D were carried out for two different obstacle geometries (rectangle and triangle) with two different heights and 5 different Reynolds numbers. Both microstructures disturbed the film flow and the interfacial length increased with higher Reynolds numbers. For the rectangular obstacle a small backflow zone was observed behind the obstacle. The successful validation and simulations enables the performance of systematic research on a wide range of geometries, phase properties and gas velocities. In the contribution, the simulations will be extended to three dimensional obstacles. This will allow the characterization of film flows even with obstacles slightly larger than the film thickness. Furthermore, a comparison to experimental results is intended.

Acknowledgments

The authors acknowledge the North-German Supercomputing Alliance (HLRN) for providing HPC resources that have contributed to the research results reported in this paper and thank the German Research Foundation (DFG) for the financial support within the project RE 1705/16-1. Furthermore, the authors thank Dr. Christian Kahle for the multiple discussions on the Cahn-Hilliard-Navier-Stokes model.

References

Abels H., Garcke H., and Grün, G., 2012, Thermodynamically consistent, frame indifferent diffuse interface models for incompressible two-phase flows with different densities, Mathematical Models and Methods in Applied Sciences 22 (3): 1150013.

Alnæs M.S., Johan H., Kirby R.C., Langtangen H.P., Logg A., Wells G.N., 2011, The FEniCS Manual, October, 196.

Balay S., Abhyankar S., Adams M., Brown J. , Brune P., Buschelman K., Eijkhout V., Gropp W., Kaushik D., Knepley M., 2014, PETSc Users Manual Revision 3.5.

Bonart H., Kahle C., Repke J.-U., Simulating Moving Contact Line Problems Using the Cahn-Hilliard-Navier-Stokes Equations, Proceedings of the FEniCS Conference 2017, Luxembourg, 12.-14. June 2017.

Bontozoglou V., Serifi K., 2008, Falling Film Flow along Steep Two-Dimensional Topography: The Effect of Inertia, International Journal of Multiphase Flow 34 (8): 734–47.

Dressaire E., Courbin L., Crest J., Stone H.A., 2010, Inertia Dominated Thin-Film Flows over Microdecorated Surfaces, Physics of Fluids 22 (7): 1–13.

Ferziger J. H., Peric M., 2002, Computational Methods for Fluid Dynamics, 3rd, Berlin, New York, Springer.

Gambaryan-Roisman T., Alexeev A., Stephan P., 2005, Effect of the Microscale Wall Topography on the Thermocapillary Convection within a Heated Liquid Film, Experimental Thermal and Fluid Science 29 (7): 765–72.

Garcke H., Hinze M., Kahle C., 2016, A Stable and Linear Time Discretization for a Thermodynamically Consistent Model for Two-Phase Incompressible Flow, Applied Numerical Mathematics 99: 151–71.

He QW., Kasagi N., 2008, Phase-Field simulation of small capillary-number two-phase flow in a microtube, Fluid Dyn Res 40(7–8):497–509.

Jacqmin D., 2000, Contact-Line Dynamics of a Diffuse Fluid Interface. Journal of Fluid Mechanics 402 (2000): S0022112099006874.

Kapoustina V., Ross-Jones J., Hitschler M., Rädle M., Repke J.-U., 2015, Direct Spatiotemporally Resolved Fluorescence Investigations of Gas Absorption and Desorption in Liquid Film Flows, Chemical Engineering Research and Design 99 (July), Institution of Chemical Engineers: 248–55.

Kohrt M., Ausner I., Wozny G., Repke J.-U., 2011, Texture Influence on Liquid-Side Mass Transfer, Chemical Engineering Research and Design 89 (8): 1405–13.

Paschke S., 2011, Experimentelle Analyse Ein- Und Zweiphasiger Filmströmungen Auf Glatten Und Strukturierten Oberflächen, PhD Thesis.

Repke J.-U., Kohrt M., Wozny G, 2011, Untersuchungen Mehrphasiger Strömungen an Einfachen Geneigten Platten Als Potenzielles Auslegungswerkzeug Für Technische Trennapparate, Chemie Ingenieur Technik 83 (7): 1107–14.

Spurk J. H., Aksel N., 2008, Fluid Mechanics, 2nd, Springer, Berlin.

Veremieiev S., Thompson H.M., Gaskell P., 2015, Free-Surface Film Flow over Topography: Full Three-Dimensional Finite Element Solutions, Computers & Fluids 122 (November). Elsevier Ltd.: 66–82.

Wörner M., 2012, Numerical Modeling of Multiphase Flows in Microfluidics and Micro Process Engineering: A Review of Methods and Applications, Microfluidics and Nanofluidics 12 (6): 841–86.